Reionization by active sources and its effects on the cosmic microwave background

Jochen Weller

Blackett Laboratory, Imperial College, Prince Consort Road, London SW7 2BZ, United Kingdom
and Department of Physics, University of California at Davis, Davis, California 95616*

Richard A. Battye

Department of Applied Mathematics and Theoretical Physics, University of Cambridge, Silver Street, Cambridge CB3 9EW,
United Kingdom

Andreas Albrecht

Blackett Laboratory, Imperial College, Prince Consort Road, London SW7 2BZ, United Kingdom
and Department of Physics, University of California at Davis, Davis, California 95616*

We investigate the possible effects of reionization by active sources on the cosmic microwave background. We concentrate on the sources themselves as the origin of reionization, rather than early object formation, introducing an extra period of heating motivated by the active character of the perturbations. Using reasonable parameters, this leads to four possibilities, depending on the time and duration of the energy input: delayed last scattering, double last scattering, shifted last scattering, and total reionization. We show that these possibilities are only very weakly constrained by the limits on spectral distortions from the Cosmic Background Explorer Far Infrared Absolute Spectrometer measurements. We illustrate the effects of these reionization possibilities on the angular power spectrum of temperature anisotropies and polarization for simple passive isocurvature models and simple coherent sources, observing the difference between passive and active models. Finally, we comment on the implications of this work for more realistic active sources, such as causal white noise and topological defect models. We show for these models that non-standard ionization histories can shift the peak in the cosmic microwave background power to larger angular scales. [S0556-2821(99)08120-5]

PACS number(s): 98.80.Cq

I. INTRODUCTION

It is well known that the angular power spectra of temperature anisotropies and polarization of the cosmic microwave background (CMB) depend sensitively on the thermal history of the universe [1–8]. Around the time of recombination ($z \approx 1100$), when protons and electrons recombine into neutral hydrogen, the microscopic physical processes at work are relatively well understood and the calculation of the photon visibility function, which feeds into the angular power spectra, is relatively simple, at least in theories with passive fluctuations, such as inflation.

However, even in these theories the universe must have become reionized, since there is no Lyman-α trough in distant quasar spectra (the Gunn-Peterson test [9]). It is thought that this must be due to virialized objects, such as protogalaxies, massive stars and quasars, which formed relatively early in the history of the universe [10–12]. The microphysics of such processes is less well understood, but photoionization due to radiative objects cannot happen earlier than when these objects have been created, which is believed to be at redshifts below $z = 100$, and it is actually thought more likely to have happened much later, after $z \approx 30$ [4,10–19]. If this is the case, then the actual observed CMB anisotropies and polarization will be a small perturbation on those calculated using the standard thermal history, just including re-

combination, due to the small optical depth of the time of reionization. Nonetheless, there are some potentially observable effects, particularly in the polarization [20].

As always the situation is much less clear in the case of actively generated perturbations, such as those from topological defects [21–23]. In such models, one is forced to try to model highly non-linear processes from the time of defect formation to the present day, which is approximately 25 orders of the magnitude in expansion. Even with the most powerful super-computers available at present, it is difficult to achieve much more than a factor of 1000 in expansion and hence extrapolations are necessary. Notwithstanding these difficulties there does seem to be a consensus at the present as to the predictions of the simplest models, cosmic strings and textures [24–26,29–31], using the standard thermal history. It appears that flat universe models with critical matter density ($\Omega_m = 1$) would require unacceptably large biases (≈ 5) on $100h^{-1}$ Mpc scales to be consistent with the observed galaxy distribution [24–26], although more exotic defect models may not have this problem [26–28]. More acceptable models can be constructed in an open universe or one dominated by a cosmological constant [29,31,32]. Even, if these models were to be ruled out by future observations, it is still important to investigate the possibility of more general active sources as the only credible alternative to inflation.

The purpose of this paper is to investigate the possible effects of the active character of such sources for structure formation on the thermal history of the universe. The basic conceptual difference between active and passive models, such as inflation, is that the sources are present in the pre-

and post-recombination plasma. This can create potentially large, local, non-linear perturbations, which can accelerate matter causing shock heating up to temperatures of a few million Kelvin in the baryons [33]. In order to perform a convincing quantitative treatment of these effects one would have to incorporate the sources accurately into a full hydrodynamic simulation which has sufficient resolution to accurately model both the activation of ionization by the gravitational effect of the sources on the smallest scales and also large enough to model the effects of an expanding universe. Obviously, the amount of computer resources required for such a simulation would be prohibitive, and so as a compromise we simply incorporate a Gaussian energy input into the thermal history calculation, which models what we believe would be the effect of a network of active sources. The *effective* influence of a network is given by a *smooth* temperature change of the baryons over a certain period of time. A simple way to introduce a smooth ''jump'' in the temperature is by an error function, so that the heating rate is a Gaussian. This model based approach allows us to investigate whether there are potentially interesting effects, before resorting to the more time consuming simulation based approach. This source has three parameters, the redshift of the maximum energy input, the amplitude at the maximum and width of the Gaussian which models the increase to and decrease from the maximum. Surprisingly, we find that the limits on the spectral distortions in the black-body spectrum of the CMB provided by the Far Infrared Absolute Spectrometer (FIRAS) instrument on the Cosmic Background Explorer (COBE) satellite, only constrain these parameters very weakly.

The thermal history calculation yields the so called photon visibility function [1], parametrized by time, which acts as a source for the linear Einstein-Boltzmann solver CMBFAST [34]. This function encodes statistical information on when the photons which we observe today were last scattered. For the standard thermal history including just recombination, it can be modeled as a Gaussian centered around $z \approx 1100$ with width $\Delta z \approx 50$. When we include the energy input there are four interesting situations which can occur. If the energy input is around or just after recombination then it is possible to modify the time and length of the last scattering epoch. If the energy input occurs once the recombination epoch is ostensibly over, and is sufficiently short for some of the photons to remain unscattered, then it is possible to have effectively two surfaces of last scattering, one around the time of recombination and the other around the time of reionization due to the energy input. If the energy input is sufficiently late for recombination to be complete, and long enough for almost all the photons observed today to be re-scattered at reionization, then it is possible for there to be a single surface of last scattering at a much lower redshift, effectively shifting the time of last scattering. Finally, if the period of heating is very late and long, then the universe remains at least partially ionized for most of the time after recombination and becomes totally ionized after $z \approx 10$. We shall describe these four possibilities as delayed, double and shifted last scattering, and total ionization in the rest of this paper. Of course none of these possibilities is totally funda-

mental and just about anything is possible for a sufficiently complicated source, but they do have some illustrative value.

In the next section, we discuss the calculation of the thermal history. First, we include a detailed review of the standard thermal history used in most linear Einstein-Boltzmann solvers. Then we introduce our topological defect motivated energy source and illustrate the different effects it can have on the thermal history of the CMB by reference to the photon visibility function. The effect of this source on the black-body spectrum of the CMB is discussed and we show that the current limits on spectral distortions would have to be substantially improved before we could exclude such thermal histories. In Sec. III, we discuss the effects of these modified thermal histories on the angular power spectra of temperature anisotropies and polarization, using simple analytic arguments to provide qualitative understanding and a linear Einstein-Boltzmann solver to give quantitative results. Finally, we discuss the possible implications for more realistic active models such as topological defects and causal white noise models. It should be noted that we have used natural units ($\hbar = k = c = 1$) throughout this paper.

II. THERMAL HISTORY CALCULATIONS

A. The standard thermal history

Originally, the thermal history of the CMB was studied using the Saha equation. This gave sensible quantitative results, which were subsequently extended by Peebles and Zel'dovich [35,36] to include various corrections due to the complexity of recombination to the ground state of hydrogen. These calculations have been further extended to include more aspects of the underlying Boltzmann equations for the photons and electrons, and calculations are now at the stage where further improvements should only lead to about 1% corrections to the angular power spectra of temperature anisotropies and polarization [8], although even further improvements [37] lead to somewhat higher than 1% corrections. In this section, we review these calculations of the standard thermal history.

We quantify the change in the number density of a particular species in terms of the relevant Boltzmann equations. Strictly, speaking there are seven equations for the protons, hydrogen, helium, singly ionized helium, doubly ionized helium, electrons and photons. However, it is sufficient to treat the helium, both singly and doubly ionized, just using the Saha equation approximation, since the recombination rate for helium is much faster than the expansion rate during the relevant epoch [38]. Also we are really only interested in the evolution of the photons and electrons since the interaction of the photons with the relatively heavy baryons is negligible. The number of photons is much larger than the electrons and therefore their evolution can be decoupled from the electrons, with this interaction being treated in terms of the spectral distortions discussed later. Hence, we can model recombination in terms of the fraction of ionized free electrons $x_e \equiv n_e^{\text{free}}/n_H$, where $n_H = n_B(1 - Y_{\text{He}})$ is the number density of hydrogen nuclei, n_B is the number density of baryons and $Y_{\text{He}} \approx 0.24$ is the mass fraction of primordial helium created at Big Bang Nucleosynthesis. In fact,

$$x_e = x_H + \frac{1}{4}\frac{Y_{He}}{1-Y_{He}}x_{He}, \qquad (1)$$

where x_H is the fraction of ionized hydrogen and x_{He} is that due to helium. Using the Saha equation, one can show that the fraction of He$^+$ is about 10^{-5} for redshifts below $z = 2000$ and for He^{++} this is even lower. Hence, x_{He} is always less than 10^{-5} and can be included simply into the calculation using only hydrogen. One slightly odd side-effect of including helium in this way is that x_e can be greater than one, although this is only the inclusion of helium modifying the calculation in the appropriate way; x_H is always one or less. The equation which governs the recombination of protons and electrons into hydrogen is

$$\frac{dx_H}{dt} = -t_{rec}^{-1} + t_{pi}^{-1} + t_{ci}^{-1}, \qquad (2)$$

with t_{rec}^{-1}, t_{pi}^{-1} and t_{ci}^{-1} being the rates for recombination of hydrogen, photoionization and collisional ionization. In the standard case, there are no external sources of photoionization and collisional ionization and, therefore, we just need to calculate the recombination rate.

However, to do this we will also need to model the evolution of the temperature of these distributions. The photon temperature is just redshifted by the expansion of the universe $T_\gamma = T_0(1+z)$ at redshift z, where $T_0 = 2.728$ K is the current temperature of the CMB, while all the other non-relativistic species remain in thermal equilibrium with each other. One can derive the evolution of the electron temperature T_e using the first law of thermodynamics [15],

$$\frac{dT_e}{dt} = -2\frac{\dot{a}}{a}T_e + \frac{2}{3}\frac{1}{1-3Y_{He}/4+(1-Y_{He})x_e}(\Gamma-\Lambda)$$
$$-\frac{1-Y_{He}}{1-3Y_{He}/4+(1-Y_{He})x_e}T_e\frac{dx_e}{dt}, \qquad (3)$$

where a is the Friedman-Robertson-Walker (FRW) scale factor, Γ is the heating rate per baryon and Λ the cooling rate per baryon. The first term on the right hand side is cooling due to expansion, the third term characterizes cooling or heating due to the change in the number of free particles. The second term is a summation of the heating and cooling rates of the physical processes involved

$$\Gamma = \Gamma_{src}, \qquad \Lambda = \Lambda_{rec} + \Lambda_{CMB}, \qquad (4)$$

where Λ_{rec} is cooling due to recombination, Λ_{CMB} is the Compton cooling from the interaction with the CMB photons and Γ_{src} is any energy input which we might postulate, assumed to be zero for the standard case. This can be further simplified by realizing that the recombination cooling due to the loss of kinetic energy from the changing number of free particles is

$$\Lambda_{rec} = \frac{3}{2}T_e(1-Y_{He})t_{rec}^{-1}. \qquad (5)$$

In the standard case, where we have no source of photoionization or collisional ionization, one can use (2) to replace t_{rec}^{-1} with dx_e/dt, which then exactly cancels the last term in (3).[1] Physically, we are just canceling off two processes which are in equilibrium. Hence, in order to calculate the standard thermal history we must just compute t_{rec}^{-1} and Λ_{CMB}, and then use a numerical routine to solve the differential equations for x_e and T_e, although the stiff nature of these differential equations does require some caution.

In order to compute these two quantities we shall now assume a flat, $\Omega_0 = 1$, universe with the Hubble parameter

$$H(a) = H_0 a^{-2}(a+a_{eq})^{1/2}, \qquad (6)$$

where $a_0 = 1$, $a_{eq} = (1+z_{eq})^{-1}$ and $z_{eq} = 2.40 \times 10^4 h^2(T_0/2.728 \text{ K})^{-4}$ is the redshift of radiation-matter equality, with the Hubble constant parametrized in the usual way, $H_0 = 100h$ km Mpc^{-1} sec^{-1}. The recombination rate that we must calculate here is the "net" rate, taking in account both the recombination and ionization rate to and from *all* states of the hydrogen atom. Recombination directly to the ground state produces a Lyman-α photon, which, with high probability, immediately ionizes a hydrogen atom, either the one which it has come from or one of its close neighbors. Hence, we do not have to consider recombination to the ground state with the exception of two possibilities. Firstly, some of the Lyman-α photons may be redshifted out of their resonance line, before they have the chance to be reabsorbed. Failing that the ground state can only be reached by the two photon decay: $2s_{1/2} \to 2p_{1/2} + \gamma \to 1s + \gamma$. The net recombination rate for transitions to and from states above the ground state and these two possibilities for the ground state is given by [35,39]

$$t_{rec}^{-1} = \alpha_e x_H n_H C - \beta_e(1-x_H)e^{-3\Delta/4T_e}C. \qquad (7)$$

This complicated expression requires some explanation. Firstly, and most simply, we define $\Delta \approx 13.60$ eV to be the binding energy of the ground state. The rate of recombination to all excited levels is [40]

$$\alpha_e = 2A\left(\frac{2T_e}{\pi m_e}\right)^{1/2}\frac{\Delta}{T_e}\phi'\left(\frac{\Delta}{T_e}\right)\bar{g}, \qquad (8)$$

where $A = 2^5 3^{-3/2}\alpha^3\pi A_0^2 = 2.105\times10^{-22}$ cm^2 given in terms of the fine structure constant $\alpha = 1/137$ and the Bohr radius $A_0 = 0.529$ Å, and $m_e = 0.511$ MeV is the electron mass. Also included is a quantum correction[2] for radiative effects known as the Gaunt factor which is given by $\bar{g} \approx 0.943$ for temperatures below 5000 K. The function $\phi'(t_e)$

---

[1]Strictly speaking the description in the text should include the effects of helium, but exactly the same cancelation will take place when this is included correctly for the same physical reasons.

[2]A more precise fitting formula for the recombination rate is given in [8]. However, the effect on the anisotropy power spectrum, by including these corrections is less than 2%.

comes from summing up the interaction cross-sections of all excited levels and is given by [40,41]

$$\phi'(t_e) = \frac{1}{2}\left(1.735 - \ln t_e + \frac{t_e}{6}\right) - \frac{1}{t_e}e^{1/t_e}E_1(1/t_e), \quad (9)$$

where

$$E_1(x) = \int_x^\infty e^{-u}/u \, du \quad (10)$$

is the exponential integral function and $t_e = T_e/\Delta$. The ionization rate β_e is related to the recombination rate by a detailed balance argument and local thermal equilibrium between all the excited states, and is given by

$$\beta_e = \alpha_e\left(\frac{m_e T_e}{2\pi}\right)^{3/2} e^{-B_2/T_e}, \quad (11)$$

with $B_2 = \Delta/4$ being the binding energy of the lowest lying excited, $n=2$, state. Finally, the correction due the redshift of Lyman-α photons and the two photon decay is [35,39]

$$C = \frac{1 + K\mathcal{D}n_{1s}}{1 + K(\mathcal{D} + \beta_e)n_{1s}}, \quad (12)$$

where $K = \lambda_\alpha^3 \dot{a}/8\pi\dot{a}$, $\lambda_\alpha = 1216$ Å is the wavelength of the Lyman-α photons, $\mathcal{D} = 8.23$ s^{-1} is the net rate of the two-photon decay and $n_{1s} \simeq (1 - x_H)n_H$ the number density of hydrogen atoms in the $1s$ state. At very late times the density of the baryons and electrons is low and direct recombination to the ground state is possible, since the density of the produced Lyman-α photons is then low as well [42]. This leads effectively to $C \to 1$ at low redshifts, where we have choosen $z < 100$. The inclusion of this effect did not change the reionization histories we studied.

In order to calculate the Compton cooling rate, one must use the Boltzmann equation for the photon distribution, which in full generality is [43–47]

$$\frac{dn}{dt}(\nu,t) = \left.\frac{\partial n}{\partial t}\right|_{cs} + \left.\frac{\partial n}{\partial t}\right|_{br} + \left.\frac{\partial n}{\partial t}\right|_{dc}, \quad (13)$$

where the subscripts refer to Compton scattering, production of bremsstrahlung (free-free) photons and double Compton scattering, respectively and ν is the frequency of the photons. We only need to concern ourselves with the term due to Compton scattering, since the other two processes lead to negligible cooling. When integrated over frequency, this gives the Compton cooling rate for Thomson scattering of hot electrons off photons in the plasma [43–45,12]

$$\Lambda_{CMB} = \frac{T_e - T_\gamma}{T_\gamma}\left(\frac{n_e^{free}\sigma_T}{\pi^2 m_e n_B}\right)\int_0^\infty \omega^4 n_{CMB}(n_{CMB} + 1)d\omega$$

$$= \frac{4\sigma_T\pi^2}{15m_e}(T_e - T_\gamma)T_\gamma^4(1 - Y_{He})x_e \quad (14)$$

$$\approx 6.232\frac{eV}{s}\left(\frac{T_e - T_\gamma}{\Delta}\right)\left(\frac{T_\gamma}{\Delta}\right)^4(1 - Y_{He})x_e,$$

where the Thomson scattering cross section is $\sigma_T = 6.65 \times 10^{-29}$ m^2 and n_{CMB} is the undistorted cosmic microwave background spectrum, $n_{CMB}^{-1} = e^{\omega/T_\gamma} - 1$.

B. The Gaussian energy input

In the previous section we reviewed the standard thermal history of the CMB. We ignored the effects of photoionization, which is usually assumed to be the source of ionization in the intergalactic medium due to early object formation, and set to zero the heating due to sources, Γ_{src}. As already stated the purpose of this paper is to investigate the possible effects of the active sources themselves and in this section we introduce a phenomenological expression for Γ_{src}, which is intended to model the effects of a network of topological defects, specifically cosmic strings. In order to do this we have to make various assumptions which basically allow us to say that the whole universe becomes ionized in an essentially homogenous way. This is unlikely to be completely true in a realistic model, since sources are random, but it is required for us to make calculations possible. The effects of inhomogeneous reionization contribute only to second order in the CMB anisotropies and will be the subject of future work.

We assume, therefore, that the active sources are distributed homogeneously in the universe and more importantly that the density of these sources is large enough that they will interact significantly with *all* the baryons over a short timescale. At early times the thermal velocity of the particles in the plasma is large and the velocity perturbations will be relatively small, so the sources will have negligible effect on the baryons. But as the perturbations grow and the thermal velocities are redshifted by expansion, the sources will become more significant. In the case of cosmic strings, it has been suggested [33] that the formation of wakes starts around $z \approx 800$, which can shock heat the plasma up to temperatures of a few million Kelvin during subsequent epochs, dependent on the small scale properties of the string network. The increasing kinetic energy of the plasma leads to a partial reionization of hydrogen, but as the density of active sources decreases, the energy release in the plasma will also decrease. Therefore, the heating takes place only over a finite period of time and afterwards the temperature of the baryons will remain constant, if, for the moment, we neglect the effects of cooling. One could model this effect in many ways and we have chosen to do this using a smooth function which interpolates between temperature of the plasma before the energy input and the temperature after heating by the sources, once again assuming no cooling. More specifically, all the baryons are heated up to a temperature of T_{heat} during a time interval of length $\Delta z = \rho$, centered around $z = \bar{z}$, using the energy per free particle per comoving volume

$$q = \frac{T_{heat}}{2}\left[1 + \frac{\sqrt{\pi}}{2}\mathrm{erf}\left(\frac{\sqrt{2}}{\rho}(z - \bar{z})\right)\right], \quad (15)$$
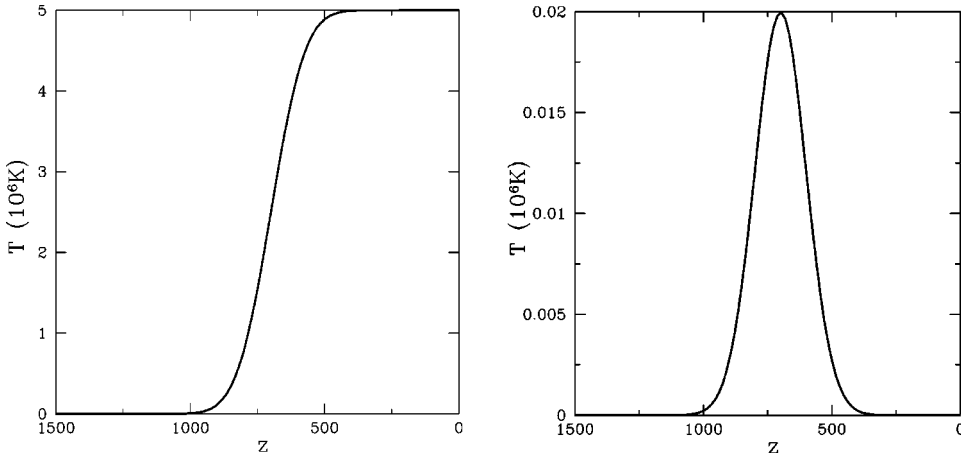
FIG. 1. An example of the energy input. On the left the energy input per free particle per comoving volume, q, as a function of redshift and on the right the corresponding rate of energy input, $-dq/dz$.

where erf(x) is the error function defined, in the standard way, by

$$\text{erf}(x) = \frac{2}{\sqrt{\pi}} \int_0^x e^{-u^2} du. \qquad (16)$$

Therefore, the rate of energy input has a Gaussian shape

$$\Gamma_{\text{src}} = \frac{3}{2} \left(1 - \frac{3}{4} Y_{\text{He}} + (1 - Y_{\text{He}}) x_{\text{e}} \right) \frac{dq}{dz} \frac{dz}{dt}$$

$$= \frac{3}{2} \sqrt{\frac{2}{\pi}} \left(1 - \frac{3}{4} Y_{\text{He}} + (1 - Y_{\text{He}}) x_{\text{e}} \right)$$

$$\times (1+z)^{5/2} \frac{H_0 T_{\text{heat}}}{\rho} \exp \left[-\frac{2}{\rho^2} (\bar{z} - z)^2 \right], \qquad (17)$$

where ρ is the width of the Gaussian, T_{heat}/ρ is proportional to its height and $\bar{z}$ is the position of the peak. The energy input (15) and the rate (17) are plotted in Fig. 1 for $\bar{z} = 700$, $\rho = 200$ and $T_{\text{heat}} = 5.0 \times 10^6$ K. We want to emphasize again that our heating model is just an ansatz, which is what we believe a reasonable one and allows one to predict the behavior of the CMB caused by such a heating process.

Of course, the plasma will never achieve these high temperatures since Compton cooling is very efficient for $z > 10$, and in fact we find that it is difficult for the actual electron temperature to get much above $T_{\text{e}} \approx 5000$ K. If the effects of the energy input are not significant at late times, then the temperature of the electrons will drop back to the CMB temperature, once the heating has stopped. However, it is possible for the electron temperature to remain around 5000 K if the energy input is significant at low redshift (see, for example, the *total ionization* model discussed below).

So we now have a source term to add to the standard thermal history which is motivated by a network of evolving topological defects. In the standard thermal history we made a number of assumptions, which need to be re-examined in the presence of this source. Firstly, there is still no source of photoionization, since ionization by free-free emissions is negligible for our shock motivated source. The addition of the source can also lead to collisional ionization, but we have

explicitly checked that this is negligible. The main reason for this is that the densities are not high enough and the fact that $\Delta \approx 13.60$ eV ≈ 158000 K is much higher than the temperature of the plasma achieved by the thermal input. Similarly we have checked that collisional ionization and excitation do not play a significant role in the cooling process since they are much weaker than Compton cooling.

Hence, we conclude that to model the effects of a topological defect network on the thermal history of the CMB, one can just modify the standard calculation by the inclusion of the source term (17) bearing in mind the uncertainties of the ansatz. One might wonder how the ionization occurs, since we have explained above that the usual physical processes—photoionization and collisional ionization—are negligible. The basic mechanism is by modifying the rates for recombination and ionization, α_{e} and β_{e} respectively, creating a shift in the balance between atomic hydrogen and free protons and electrons. More specifically, the increase in T_{e} creates a significant modification to α_{e} (the probability that an electron is captured by a proton decreases with increasing T_{e}) and a slightly smaller effect in β_{e}, reducing t_{rec}^{-1}, hence shifting the balance towards free protons and electrons. In other words, ionization dominates over recombination as long as the matter temperature is large.

We have investigated the effects of using this source for a wide range of parameters and found that there are four cases which can illustrate interesting effects. We call them *delayed*, *double* and *shifted* last scattering, and *total ionization* and an example of each is discussed below. Before doing this we should discuss what we shall use to quantify their effect on the microwave background. The differential optical depth due to Thomson scattering is $\dot{\tau} = x_{\text{e}} n_{\text{H}} \sigma_{\text{T}} a$ and hence the optical depth of any particular conformal time η is

$$\tau(\eta) = \int_\eta^{\eta_0} \dot{\tau}(\eta') d\eta', \qquad (18)$$

where η_0 is the conformal time of the present day. From these two quantities we can construct two photon visibility functions [1], the last scattering visibility function

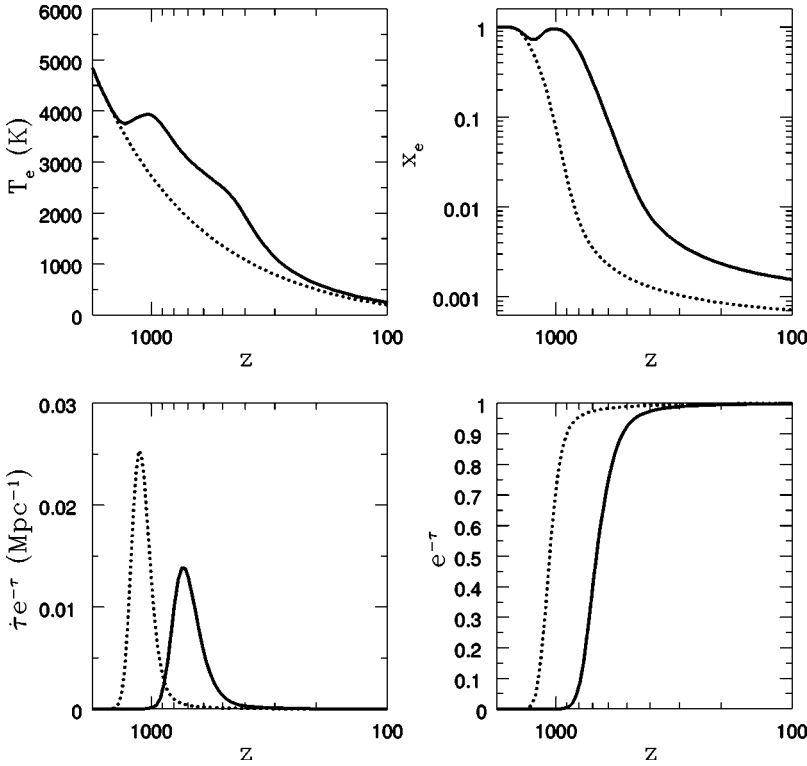$$g(\eta) = \dot{\tau}(\eta) e^{-\tau(\eta)}, \qquad (19)$$

FIG. 2. The effects of *delayed* last scattering on the thermal history and photon visibility functions. We have used $\bar{z} = 1000$, $\rho = 350$ and $T_{heat} = 1.3 \times 10^8$ K. The plots are (top, left) the electron temperature T_e; (top, right) the fraction of ionized electrons x_e; (bottom, left) the last scattering visibility function; (bottom, right) the cumulative visibility function, all plotted against redshift z. On each plot there are two curves, the modified (solid line) and standard (dotted line) thermal histories.

and the cumulative visibility function

$$h(\eta) = e^{-\tau(\eta)}, \tag{20}$$

which encode statistical information about when the CMB photons observed today were last scattered or influenced by objects, such as topological defects, along the line of sight. We have already commented that in the standard thermal history the last scattering visibility function is a Gaussian of width $\Delta z \approx 50$ centered around $z \approx 1100$. The cumulative visibility function is even simpler, being effectively zero for $z > 1100$ and increasing sharply to one for $z < 1100$ in the standard case. This reflects our inability to see directly any objects beyond the surface of last scattering since the universe is opaque. It also has a simple statistical interpretation; for any given conformal time η, then $h(\eta)$ is the probability that a given photon was scattered before η and $1 - h(\eta)$ is the probability that it was scattered after η. We shall see that these functions occur naturally in the calculation of CMB anisotropies and hence it is important for us to understand the effects of our energy input on them.

Delayed last scattering. If the energy input is significant during or close to the epoch of recombination then it is possible to delay standard recombination. An example of this is $\bar{z} = 1000$, $\rho = 350$ and $T_{heat} = 1.3 \times 10^8$ K, whose effects on the thermal history and photon visibility functions are illustrated in Fig. 2. We see that the temperature of the electrons deviates away from that of the photons around $z \approx 1500$ and only manages to get back down to be close to the photon temperature around $z \approx 100$. This allows a significant delay in recombination process with the ionization fraction remaining greater than 70% until around $z \approx 700$. The last scattering

visibility function is still similar to a Gaussian, but it peaks around $z \approx 700$, as opposed to $z \approx 1100$, with a larger width and consequentially smaller amplitude. A corresponding change in the cumulative visibility function is also observed, with the transition from zero to one happening around $z \approx 700$.

Double last scattering. If the energy input is slightly later, then it is possible for recombination to take place in the standard way, with x_e decreasing almost to zero before increasing once again as the electron temperature begins to rise due to the energy input. If the period of heating is short enough for a substantial fraction of the photons which were originally last scattered at the standard time to remain unscattered during the reionized epoch, then it is possible to have effectively two surfaces of last scattering. This can be achieved, for example, if $\bar{z} = 500$, $\rho = 100$ and $T_{heat} = 10^7$ K, and its effects are compared to the standard case in Fig. 3. As for *delayed* last scattering the electron temperature deviates significantly from that photon temperature, but now it takes place over a relatively short timescale, between $z \approx 700$ and $z \approx 300$. The first epoch of recombination is effectively over by around the time at which T_e begins to increase, but this increase leads to ionization which reaches a maximum of around 30% by $z \approx 450$, before decreasing again. The last scattering visibility function can be approximated by two Gaussians one centered around $z \approx 1100$ and the other around $z \approx 500$. The cumulative visibility function has two steps, from zero to 0.3, and then from 0.3 to one. This tells us that 30% of the photons observed today were last scattered around the time of standard recombination, while the other 70% were last scattered during the epoch of reionization.
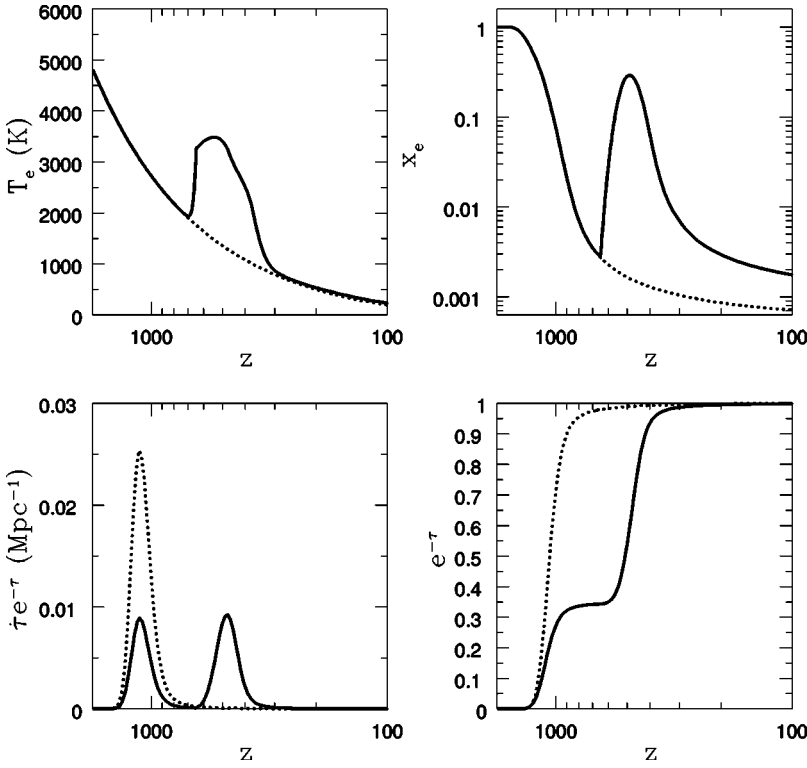
FIG. 3. The effects of *double* last scattering using $\bar{z}=500$, $\rho=100$ and $T_{\mathrm{heat}}=10^7$ K. The plots are arranged in the same order as Fig. 2.

Shifted last scattering. If the energy input takes place after the standard recombination has taken place, as for *double* last scattering, but the duration for which it takes place is much longer, then most of the CMB photons will be re-scattered during the epoch of reionization and the photon visibility function will be almost zero around the time of standard recombination. Although, this is physically distinct from *delayed* last scattering, the photon visibility functions will be very similar apart from a shift to lower redshift, and hence we call this *shifted* last scattering. Using $\bar{z}=500$, $\rho=200$ and $T_{\mathrm{heat}}=4\times10^7$ K, one can shift the surface of last scattering to lower redshift, as illustrated in Fig. 4. In this case, the electron temperature is above that of the photons from around $z\approx800$ until very close to the present day (z
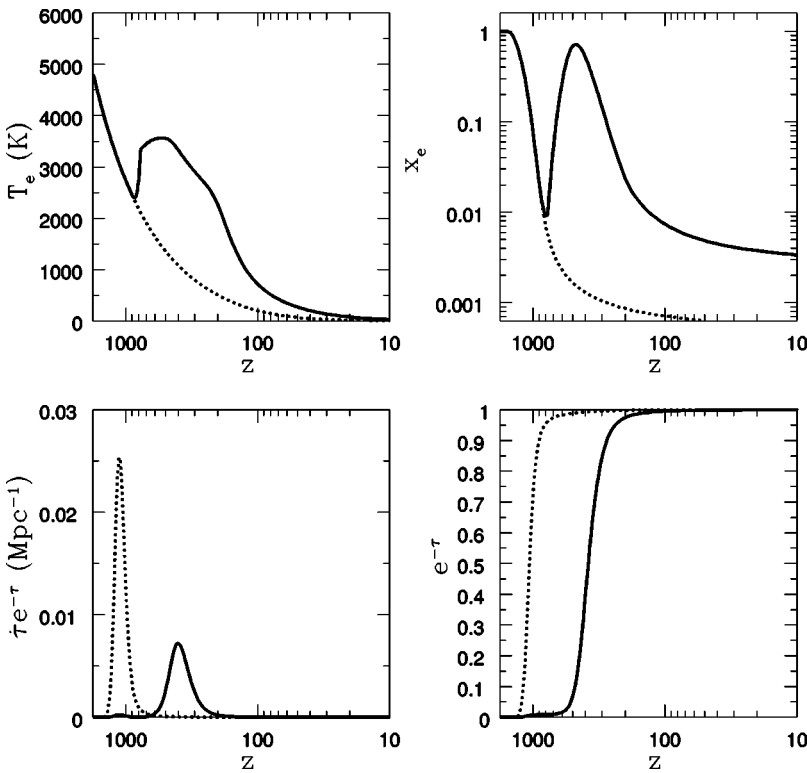

FIG. 4. The effects of *shifted* last scattering using $\bar{z}=500$, $\rho=200$ and $T_{\mathrm{heat}}=4\times10^7$ K. The plots are arranged in the same order as Fig. 2.
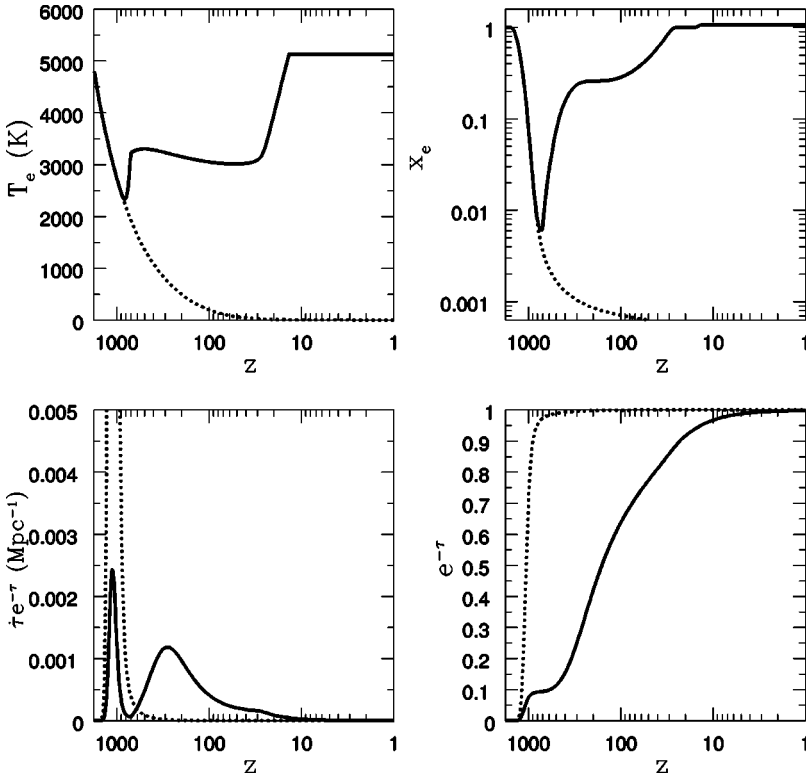
FIG. 5. The effects of *total ionization* using $\bar{z}=350$, $\rho=300$ and $T_{\text{heat}}=1.5\times10^7$ K. The plots are arranged in the same order as Fig. 2.

≈10), with the fraction of free electrons being larger than 10% between $z\approx700$ and $z\approx100$. The last scattering visibility function is now approximately a single Gaussian centered around $z\approx500$, with a much larger width than in the standard case. The cumulative visibility function can be approximated by a single step at $z\approx500$, re-enforcing the fact that almost all the photons were last scattered during the epoch of reionization.

Total ionization. If the energy input is very late and over a substantial period then it is very difficult for the universe to become neutral to any great degree between the epoch of standard recombination and the present day. In this case, the photon visibility function will be relatively small since a large fraction of the CMB photons observed today have not stopped scattering through the whole history of the universe and effectively there is no well defined concept of last scattering. One interesting side effect of this is that the universe becomes totally ionized at around $z\approx10$ and the electron temperature does not come back down to the photon temperature, remaining at around 5000 K. An example of this type of thermal history is given in Fig. 5 using $\bar{z}=350$, $\rho=300$ and $T_{\text{heat}}=1.5\times10^7$ K. The electron temperature is much higher than the photon temperature for $z<700$, where the energy input becomes significant, and remains around 3000 K until around $z\approx20$. At this point the effects of Compton cooling reduce substantially and the electron temperature increases to be greater than 5000 K for $z<10$. There is a corresponding two step increase in the fraction of free electrons. The last scattering visibility function is much smaller than in all the other cases, but still has a peak around the time of standard recombination and a broader peak across a wide range of redshifts. The cumulative visibility function

increases from zero to about 0.1 around the epoch of standard recombination and then increases very slowly to one between $z\approx500$ and $z\approx1$. Hence, only 10% of the photons observed today were last scattered during the epoch of standard recombination and the other 90% were scattered at some point after $z\approx500$. The amount of energy per baryon injected into the universe is given by $E/N_{\text{b}}=3/2T_{\text{heat}}$, which gives in the case of *delayed last scattering* 16.8 keV per baryon. After the baryons reach equilibrium with the CMB this energy input is recognizeable as spectral distortion of the Planckian spectrum which is discussed in the next subsection. The resulting distortions should be small since there are about 10^9 photons per baryon.

We should emphasize that none of these possibilities is fundamental and the effects described above will often be superposed in a non-trivial way. Also only the *total ionization* model achieves substantial ionization at late times and hence some other mechanism, probably photoionization, would be required to pass the Gunn-Peterson test.

Although the mechanisms of heating and reionization discussed in this paper are entirely different, the results can look very similar to reionization due to the presence of light supersymmetric particles (e.g. a light photino or higgsino) [48,49]. These light inos decay into UV-photons which subsequently ionize the matter. Dependent on the lifetime of light inos the (re-)ionization history is comparable to the one discussed in the present paper. The remaining energy of the ionizing photons can heat the matter to much larger temperatures as in the cases discussed here [49]. Other mechanism of reionization which have been studied in the past are reionization by decaying massive neutrinos [50–52] or the evaporation of primordial black holes [5,53]. It should be noted
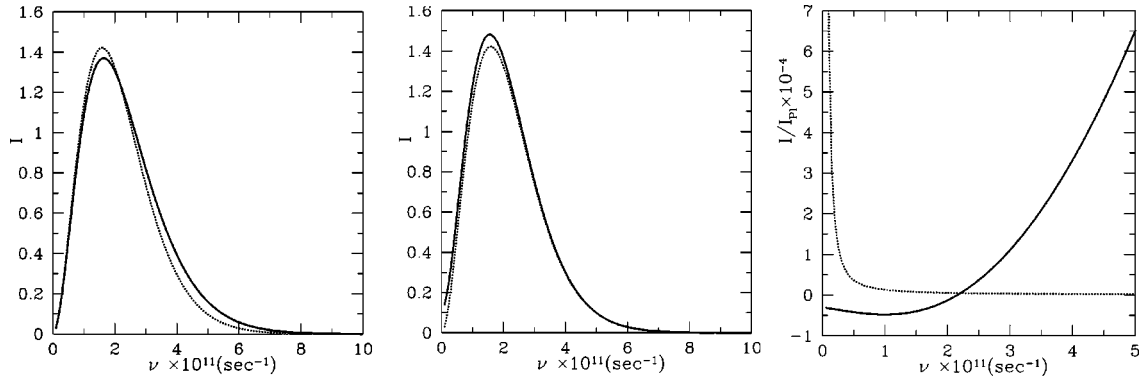
FIG. 6. On the left a y-distorted (solid line) and a Planckian (dotted line) spectrum are plotted, where it can be seen that the photons are redistributed from lower frequencies, to higher frequencies. In the middle a free-free distorted spectrum (solid line) is plotted where the increased number of low-frequency photons is established. On the right the distortions with the value of the upper limits from the COBE FIRAS experiment are plotted (solid line y-distortion, dotted line free-free distortion) relative to the related Planckian spectrum [$(n - n_{Pl})/n_{Pl}$].

that these mechanisms can also lead to reionization histories similar to the ones presented in this paper.

C. Spectral distortions

We have already noted that the number of photons is so much larger than the number of baryons and hence the evolution of the photon spectrum can be decoupled from the evolution of the number density of free electrons during standard recombination and subsequent epochs of reionization. But the spectrum does evolve and, assuming the deviations from a pure black-body are small, as they will be for cases under consideration here, the evolution of the spectrum can be studied in terms of the spectral distortions, known as the Compton y-parameter or y-distortion [44,46,54,55], the free-free distortion [56,57] and the μ-distortion [44,46,58]. The COBE satellite had on board an instrument, known as FIRAS, which measured the spectrum of the CMB to high degree of accuracy, placing apparently stringent upper bounds on these distortions. Subsequently, it was shown these upper bounds placed constraints on energy input at epochs before the standard time of recombination, but as we will show they place only very weak limits on the type of energy input that we have discussed in the previous section.

The source of energy input we have introduced will only lead to free-free and y-distortions, with the μ-distortion zero, if there is no significant energy input before the time of standard recombination, since the rate of Compton scattering is much slower than the expansion at these redshifts [61]. Similarly, we can ignore double Compton scattering relative to single Compton scattering after recombination [61]. Hence, we need only consider the y-distortion and the free-free distortion. Compton scattering conserves the total number of photons and hence the only way to increase the energy of the radiation due to the interaction with the hot plasma is by redistributing the photons from lower frequencies to higher frequencies. This is measured using the y-distortion. The thermal bremsstrahlung process on the other hand produces photons in the low frequency region, creating the free-free distortion. If the temperature is measured in the Rayleigh-

Jeans part of the spectrum, it deviates due to the increased/decreased number of photons in this part of the spectrum by [44,59]

$$\frac{T_{RJ}(x) - T_0}{T_0} = -2y,$$

$$\frac{T_{RJ}(x) - T_0}{T_0} \simeq \frac{Y_{ff}}{x^2}, \quad (21)$$

where $T_{RJ}(x)$ is the Rayleigh-Jeans temperature and T_0 is the measured temperature of the Planckian distribution.

The COBE FIRAS limits [60] on these two parameters are $|y| < 1.5 \times 10^{-5}$ (95% C.L.) and $|Y_{ff}| < 1.9 \times 10^{-5}$ (95% C.L.). In Fig. 6 (left) we have plotted the brightness I [$I \propto x^3 n(x)$, with $x \propto \nu/T$] of a spectrum with $y = 1.5 \times 10^{-2}$. The redistribution of low frequency photons to higher frequencies, due to the interaction with the hot plasma, is evident from this graph. In Fig. 6 (middle) the brightness of a spectrum with a distortion due to the release of bremsstrahlung photons from the plasma is shown, with $Y_{ff} = 0.1$. Note that the distorted graph in Fig. 6 (middle) is only valid in the Rayleigh-Jeans limit. However, one can see the increasing brightness due to extra photons in the low frequency region. Figure 6 (right) shows the relative distortion of the brightness, $I_{rel} = [I(x) - I^{Pl}(x)]/I^{Pl}(x)$ where $I^{Pl}(x)$ is the brightness of the Planckian spectrum. The values of the distortions in this plot are taken from the upper limits from the COBE FIRAS experiment.

The creation of spectral distortions is dictated by the photon Boltzmann equation (13) sourced by the Kompaneets term for Compton scattering [43–46]

$$\left.\frac{\partial n}{\partial t}\right|_{cs} = n_e^{free} \sigma_T \frac{T_\gamma}{m_e} \frac{1}{x^2} \frac{\partial}{\partial x}\left(x^4\left[\frac{T_e}{T_\gamma}\frac{\partial n}{\partial x} + n(1+n)\right]\right), \quad (22)$$

and free-free bremsstrahlung via [43,46]

$$\left.\frac{\partial n}{\partial t}\right|_{\mathrm{br}} = \kappa \frac{e^{-x_p}}{x^3}[1 - n(e^{x_p} - 1)], \tag{23}$$

where $x = 2\pi\nu/T_\gamma$ and $x_p = 2\pi\nu/T_\mathrm{e}$ are dimensionless frequencies relative to T_γ the unperturbed temperature of the CMB and the electron temperature T_e. The coefficient κ is given by

$$\kappa = \frac{32\pi^3 e^6 n_\mathrm{e}^{\mathrm{free}} n_\mathrm{B} g_\mathrm{br}(x_p)}{3 m_\mathrm{e} T_\gamma^3 \sqrt{6\pi m_\mathrm{e} T_\mathrm{e}}}, \tag{24}$$

for a plasma containing both hydrogen and helium [61] and $g_\mathrm{br}(x_p)$ is a Gaunt factor, accounting for quantum corrections to the free-free radiation process. One can either use a frequency averaged Gaunt factor $g_\mathrm{br}(x_p) = \bar{g}_\mathrm{br} \approx 1.2$ which gives an error less than 20% [62], or a more precise definition $g_\mathrm{br}(x_p) = \sqrt{3}\ln(2.25/x_p)/\pi$ for $x_p \lesssim 0.37$ and $g_\mathrm{br}(x_p) = 1$ for $x_p \gtrsim 0.37$ [61].

To account for the distortions in the black-body spectrum, we solve the Boltzmann equation in terms of the unperturbed spectrum $n_0(x)$ and the spectral distortions y or Y_ff, that is, $n(x) = n_0(x) + yf(x)$, where [44]

$$f(x) = \frac{xe^x}{(e^x - 1)^2}\left(\frac{x}{\tanh(x/2)} - 4\right). \tag{25}$$

If we do this in an $\Omega = 1$ universe then the y distortion is given by

$$y \equiv \int_{t_0}^{t_\mathrm{h}} \sigma_\mathrm{T} n_\mathrm{e}^{\mathrm{free}}\left(\frac{T_\mathrm{e} - T_\gamma}{m_\mathrm{e}}\right)dt$$

$$\approx 1.16 \times 10^{-11}\Omega_\mathrm{b} h(1 - Y_\mathrm{He})\int_0^{z_\mathrm{h}}\left(\frac{T_\mathrm{e} - T_\gamma}{1\ \mathrm{K}}\right)x_\mathrm{e}(z)$$

$$\times (1 + z)^{1/2}dz, \tag{26}$$

and the free-free distortion is given by [59]

$$Y_\mathrm{ff} \equiv \int_{t_0}^{t_\mathrm{h}} \kappa \frac{T_\mathrm{e} - T_\gamma}{T_\mathrm{e}}dt \approx 2.33 \times 10^{-6}\bar{g}_\mathrm{br}\Omega_\mathrm{b}^2 h^3(1 - Y_\mathrm{He})$$

$$\times \int_0^{z_\mathrm{h}}\left(1 - \frac{T_0}{T_\mathrm{e}}(1 + z)\right)\left(\frac{T_\mathrm{e}}{1\ \mathrm{K}}\right)^{-1/2}x_\mathrm{e}(z)(1 + z)^{1/2}dz, \tag{27}$$

where t_h and z_h are the time and redshift when the energy input becomes significant.

One can estimate an upper bound on the distortions due to our energy input, assuming that we achieve total ionization, that is, $x_\mathrm{e} = 1$ and a constant temperature, T_e over a finite range, say $z = z_\mathrm{h}$ to $z = 0$, with $z_\mathrm{h} \gg 1$. We find that the y-distortion is given by [11]

$$y \approx 2.3 \times 10^{-5}\left(\frac{\Omega_\mathrm{b}}{0.05}\right)\left(\frac{h}{0.5}\right)\left(\frac{1 - Y_\mathrm{He}}{0.76}\right)\left(\frac{T_\mathrm{e}}{5000\ \mathrm{K}}\right)\left(\frac{z_\mathrm{h}}{1000}\right)^{3/2}, \tag{28}$$

and the free-free distortion is [59]

$$Y_\mathrm{ff} \approx 6.3 \times 10^{-12}\left(\frac{\bar{g}_\mathrm{br}}{1.2}\right)\left(\frac{\Omega_\mathrm{b}}{0.05}\right)^2\left(\frac{h}{0.5}\right)^3\left(\frac{1 - Y_\mathrm{He}}{0.76}\right)$$

$$\times \left(\frac{T_\mathrm{e}}{5000\ \mathrm{K}}\right)^{-1/2}\left(\frac{z_\mathrm{h}}{1000}\right)^{3/2}. \tag{29}$$

Since our heating model does not result in larger values than $T_\mathrm{e} = 5000$ K, it is easy to see that it would be difficult to achieve much more than $y \approx 10^{-5}$ and $Y_\mathrm{ff} \approx 10^{-7}$ using standard cosmological parameters and therefore, the limits on spectral distortions from FIRAS do not constrain our model to any great degree. In fact, the actual spectral distortions are likely to be smaller than the upper bounds (28) and (29) since the ionization fraction and electron temperature are at their maxima only for a small portion of the range. We have calculated these distortions for the four models which we have been considering. They are $y \approx 3.2 \times 10^{-6}$ and $Y_\mathrm{ff} \approx 4.3 \times 10^{-8}$ for *delayed* last scattering, $y \approx 3.0 \times 10^{-7}$ and $Y_\mathrm{ff} \approx 5.2 \times 10^{-9}$ for *double* last scattering, $y \approx 1.7 \times 10^{-6}$ and $Y_\mathrm{ff} \approx 2.6 \times 10^{-8}$ for *shifted* last scattering, and finally $y \approx 9.8 \times 10^{-7}$ and $Y_\mathrm{ff} \approx 1.6 \times 10^{-8}$ for *total ionization*. For comparable heating temperatures these are also the approximate distortions given in [11,59], however [59] does not consider a particular model for the heat input. The heating temperatures in the model used in [11] are higher than the ones discussed in this paper, resulting in much stronger limitations when reionization can occur. Similar results are obtained in [44,63] under the assumption of stationary heating. Future measurements of the cosmic microwave background spectrum, like the experiments on the satellite missions MAP (Microwave Anisotropy Probe) [64], Planck Surveyor [65,66] and DIMES (Diffuse Microwave Emission Survey) [67,68], are at the level of 0.1% accuracy and can provide more stringent bounds on the distortions and could rule out some of the models discussed here. However this depends on how accurately one can remove the galactic dust contamination from the data [69].

III. ANGULAR POWER SPECTRA OF TEMPERATURE ANISOTROPIES AND POLARIZATION

A. Simple analytic arguments

To predict CMB anisotropies one has to solve the evolution equation for each species of particles either numerically [2,3,34,70,71] or analytically [72–76]. One can understand the qualitative structure of temperature anisotropies and polarization using a formalism first applied to passive adiabatic models [77–80] and later adapted to incorporate active source models [81–83]. For the purpose of this section we shall ignore the vector and tensor contributions to the anisotropies, and concentrate on the scalar component since it is this which is most affected by the modifications to the thermal history discussed earlier. In this case, the angular

power spectra for the temperature anisotropies, C_l^T, and the polarization,[3] C_l^E are given by [77,79]

$$C_l^T = \frac{2}{\pi} \int_0^\infty k^2 dk \langle \Delta_l(k,\eta_0)\Delta_l^*(k,\eta_0) \rangle,$$

$$(30)$$

$$C_l^E = \frac{2}{\pi} \int_0^\infty k^2 dk \langle E_l(k,\eta_0)E_l^*(k,\eta_0) \rangle,$$

where $\Delta(k,\eta_0,\mu)$ and $E(k,\eta_0,\mu)$ are the temperature and polarization distribution functions expanded in terms of spherical harmonics of the angular variable $\mu = \cos\theta$, with coefficients $\Delta_l(k,\eta_0)$ and $E_l(k,\eta_0)$. The basic procedure involves writing these multipoles in terms of an integral over the lower multipoles and the gravitational potentials along the line of sight.

The line of sight integral for the temperature anisotropies is then [77]

$$\Delta_l(k,\eta_0) = \int_0^{\eta_0} d\eta (S_T^0(k,\eta)j_l[k(\eta_0-\eta)]$$

$$+ S_T^1(k,\eta)j_l^{10}[k(\eta_0-\eta)]$$

$$+ S_T^2(k,\eta)j_l^{20}[k(\eta_0-\eta)]),$$

$$(31)$$

where

$$j_l^{10}(x) = j_l'(x), \quad j_l^{20}(x) = [3j_l''(x)+j_l(x)]/2,$$

$$S_T^0(k,\eta) = g(\eta)(\Delta_0+\Psi) + h(\eta)(\dot\Psi-\dot\Phi),$$

$$S_T^1(k,\eta) = g(\eta)V_B, \quad S_T^2(k,\eta) = g(\eta)P,$$

$$(32)$$

Ψ,Φ are the gravitational potentials characterizing the effects of the sources, V_B is the baryon velocity and $P = (\Delta_2 - E_2)/2$. The equivalent expression for the electric component of the polarization distribution is [80,84]

$$E_l(k,\eta_0) = -\sqrt{6} \int_0^{\eta_0} d\eta g(\eta)P(k,\eta)\epsilon_l[k(\eta_0-\eta)],$$

$$(33)$$

where

$$\epsilon_l(x) = \sqrt{\frac{3}{8}\frac{(l+2)!}{(l-2)!}}\frac{j_l(x)}{x^2}.$$

$$(34)$$

For the standard thermal history the last scattering visibility function can be approximated for pedagogical purposes by a delta function at η_* and the cumulative visibility function by a step function at the same point, that is, $g(\eta) = \delta(\eta-\eta_*)$ and $h(\eta) = \Theta(\eta-\eta_*)$. Hence, (31) and (33) can be approximated by [77,80]

$$\Delta_l(k,\eta_0) = (\Delta_0+\Psi)(k,\eta_*)j_l[k(\eta_0-\eta_*)]$$

$$+ V_B(k,\eta_*)j_l^{10}[k(\eta_0-\eta_*)]$$

$$+ P(k,\eta_*)j_l^{20}[k(\eta_0-\eta_*)]$$

$$+ \int_{\eta_*}^{\eta_0} d\eta(\dot\Psi-\dot\Phi)j_l[k(\eta_0-\eta)], \quad (35)$$

and

$$E_l(k,\eta_0) = -\sqrt{6}P(\eta_*)\epsilon_l[k(\eta_0-\eta_*)]. \quad (36)$$

Therefore, one can investigate the qualitative nature of the anisotropies and polarization by estimating $\Delta_0+\Psi$, V_B and P around the time of last scattering[4] and $\dot\Psi-\dot\Phi$ along the line of sight.

We shall primarily be interested in the contribution from acoustic oscillations, since it is they which are most sensitive to the ionization history. Using the tight coupling approximation, that is, an expansion in powers of $1/\dot\tau$, one can deduce that [77]

$$\hat\Delta_0(\eta_*) = \Delta_0(\eta_*) + \Phi(\eta_*)$$

$$= e^{-k^2/k_s^2(\eta_*,0)}\hat\Delta_0(0)\cos\left(\frac{k\eta_*}{\sqrt{3}}\right)$$

$$+ \frac{\sqrt{3}}{k}\dot{\hat\Delta}_0(0)\sin\left(\frac{k\eta_*}{\sqrt{3}}\right)$$

$$+ \sqrt{\frac{3}{k}}\int_0^{\eta_*} d\eta' e^{-k^2/k_s^2(\eta_*,\eta')}$$

$$\times \sin\left(\frac{k}{\sqrt{3}}(\eta_*-\eta')\right)F(\eta'), \quad (37)$$

where we have ignored the effects of baryons, $F(\eta) = k^2(\Phi-\Psi)/3$ is the structure function of the source,

$$k_s^{-2}(\eta_2,\eta_1) = \frac{4}{27}\int_{\eta_1}^{\eta_2} \frac{d\eta}{\dot\tau(\eta)}, \quad (38)$$

is the damping length due to photon diffusion [1,80,88] and $\hat\Delta_0(\eta) \equiv \Delta_0(\eta) + \Phi(\eta)$. This serves as an approximation for the intrinsic anisotropy created around the time of recombination. Furthermore, the other important quantities V_B and P are related to $\hat\Delta_0$ by $P \sim V_B \sim \Delta_1 \sim \dot{\hat\Delta}_0$ around this time.

With a few subtleties, the three parts to the tight coupling solution (37) correspond to the passive adiabatic $[\dot{\hat\Delta}_0(0) = 0, F(\eta) = 0]$, passive isocurvature $[\hat\Delta_0(0) = 0, F(\eta) = 0]$ and active sources $[\hat\Delta_0(0) = 0, \dot{\hat\Delta}_0(0) = 0]$. When all the rel-

---

[3]Note that since we have ignored the vector and tensor components of the source, there is no magnetic component of the polarization [87].

[4]In fact, we will calculate the $\Delta_0+\Phi$ around the time of last scattering and assume that $\Psi-\Phi$ is small.

evant effects are taken into account the contribution from V_B is suppressed relative to that from $\Delta_0 + \Psi$, and that from P is even further suppressed. Therefore, there are in general two oscillatory components to the temperature anisotropy which are out of phase with each other, one which gives rise to peaks, $\Delta_0 + \Psi$, and the other which fills in between them creating troughs, V_B. These arguments lead to the much discussed *acoustic peaks* in the standard adiabatic scenario, which has the first peak at around $l = 200$ corresponding to the size of the sound horizon at time of recombination. Isocurvature and active source models also have similar peak structures,[5] albeit with the main peak at slightly larger l [89]. The effective source of polarization Δ_1 is out of phase with that for the peaks in the anisotropy spectrum and there is no contribution to the polarization from their source, $\Delta_0 + \Psi$. This leads to a set of tight peaks which are out of phase with those for anisotropy. The amplitude of the polarization is generally much lower than the anisotropy since no net polarization is created during the tight coupling epoch [1,3,34,84,85]. We wish to modify this simple qualitative treatment of the structure of the anisotropies to the case where we have a more complicated ionization history. In order to do this, we replace the last scattering visibility function by [20,86]

$$g(\eta) = e^{-\tau(\eta_r)}\delta(\eta - \eta_*) + (1 - e^{-\tau(\eta_r)})\delta(\eta - \eta_r),$$
(39)

where η_r is the time of reionization. Using this one can deduce that the cumulative visibility function will be given by $h(\eta) = 0$ for $\eta < \eta_*$, $h(\eta) = e^{-\tau(\eta_r)}$ for $\eta_* < \eta < \eta_r$ and $h(\eta) = 1$ for $\eta > \eta_r$. This is similar to the case of *double* last scattering discussed in the previous section which is the most general case. However, we shall discuss how this approach can be modified to understand the effects of the *shifted* and *delayed* last scattering scenarios. Since the visibility functions are not well represented in this way for the case of the *total ionization* scenario, we shall only comment briefly on its effects in this section.

Using (39) we can deduce that [20]

$$\Delta_l(k,\eta_0) = e^{-\tau(\eta_r)}\{(\Delta_0 + \Psi)(k,\eta_*)j_l[k(\eta_0 - \eta_*)]$$
$$+ V_B(k,\eta_*)j_l^{10}[k(\eta_0 - \eta_*)] + P(k,\eta_*)j_l^{20}$$
$$\times [k(\eta_0 - \eta_*)]\} + (1 - e^{-\tau(\eta_r)})\{(\Delta_0 + \Psi)$$
$$\times (k,\eta_r)j_l[k(\eta_0 - \eta_r)] + V_B(k,\eta_r)j_l^{10}$$
$$\times [k(\eta_0 - \eta_r)] + P(k,\eta_r)j_l^{20}[k(\eta_0 - \eta_r)]\}$$
$$+ e^{-\tau(\eta_r)}\int_{\eta_*}^{\eta_r} d\eta(\dot{\Psi} - \dot{\Phi})j_l[k(\eta_0 - \eta)]$$
$$+ \int_{\eta_r}^{\eta_0} d\eta(\dot{\Psi} - \dot{\Phi})j_l[k(\eta_0 - \eta)].$$
(40)

---

[5] We are only considering coherent active source models at this stage.

The first term in curly brackets is due to photons which were last scattered at the time of recombination. Only a fraction $e^{-\tau(\eta_r)}$ of the total number of photons observed today will have not scattered since that epoch and the remainder, a fraction $1 - e^{-\tau(\eta_r)}$, was scattered at the time of reionization. The effect of these photons on the temperature anisotropy is given by the second term. The final two terms are a similarly modified version of the integrated Sachs-Wolfe (ISW) effect.

We have already estimated the effects of $\Delta_0 + \Psi$ and V_B at the time of recombination, and these are just damped by the factor $e^{-\tau(\eta_r)}$ in these scenarios. However, we must now also estimate their effects at the time of reionization. We assume that the photons free stream from the time of recombination until just before reionization at time $\eta_r - \epsilon$, where ϵ is usually small when compared to η_r. This yields

$$\Delta_0(\eta_r - \epsilon, k) = (\Delta_0 + \Psi)(k,\eta_*)j_0[k(\eta_r - \epsilon - \eta_*)]$$
$$+ \int_{\eta_*}^{\eta_r - \epsilon} d\eta(\dot{\Psi} - \dot{\Phi})j_0[k(\eta_r - \epsilon - \eta)].$$
(41)

If we now assume that the ISW component to this is negligible, as it will be in most applications, then this simple multiplication can be used as an initial condition for the epoch when the photons re-enter the phase where the photons couple again to the electrons. Using (37), one can deduce that [20]

$$\hat{\Delta}_0(\eta_r) = \Delta_0(\eta_r) + \Phi(\eta_r)$$
$$= e^{-k^2/k_s^2(\eta_r,\eta_r - \epsilon)}\left[\hat{\Delta}_0(\eta_r - \epsilon)\cos\left(\frac{k\epsilon}{\sqrt{3}}\right)\right.$$
$$\left. + \frac{\sqrt{3}}{k}\dot{\hat{\Delta}}_0(\eta_r - \epsilon)\sin\left(\frac{k\epsilon}{\sqrt{3}}\right)\right]$$
$$+ \sqrt{\frac{3}{k}}\int_{\eta_r - \epsilon}^{\eta_r} d\eta' e^{-k^2/k_s^2(\eta_r,\eta')}$$
$$\times \sin\left(\frac{k}{\sqrt{3}}(\eta_r - \eta')\right)F(\eta').$$
(42)

Computing V_B and P around the time of reionization is more tricky since there is pre-existing anisotropy. If this is large then it can modify the relation between V_B, P and Δ_1. We do not believe that this will have a substantial effect on the temperature, but we shall return to this point when we discuss polarization below.

We are now in a position to discuss the effects of this *double* last scattering scenario on the CMB anisotropies. The fact that there are two last scattering surfaces will lead to two sets of peaks with relative amplitudes $e^{-\tau(\eta_r)}$ and $1 - e^{-\tau(\eta_r)}$, whose scales will be set by the sound horizons at the time of recombination ($k_* \sim \eta_*^{-1}$) and the time of reionization. By substituting the free-streamed tight coupling solution into (42), one can deduce that this scale is $k_r \sim (\eta_* + \epsilon)^{-1}$, which implies that the size of the sound horizon is

proportional to the time for which acoustic oscillations take place. Remember that ϵ is small relative to η_r, but so long as $\eta_r \gg \eta_*$, then it is possible for $\epsilon \sim O(\eta_*)$, creating peaks which are based around very different scales. These scales can be projected into l-space [77] using the fact that the spherical Bessel function $j_l(x)$ is peaked around $x = l$, which in the case of the anisotropy created at the time of last scattering is $l \approx k_*(\eta_0 - \eta_*)$ and for that created at reionization is $l \approx k_r(\eta_0 - \eta_r)$.

This qualitative approach can be modified to also explain the nature of the structure of the anisotropy in the *shifted* last scattering scenario. In this case, the optical depth of the reionization is very large, $\tau(\eta_r) \gg 1$, which implies that one can ignore the first term in (40), and hence the anisotropy is given by

$$\Delta_l(k, \eta_0) = (\Delta_0 + \Psi)(\eta_r) j_l[k(\eta_0 - \eta_r)]$$
$$+ V_B(\eta_r) j_l^{10}[k(\eta_0 - \eta_r)] + P(\eta_r) j_l^{20}[k(\eta_0 - \eta_r)]$$
$$+ \int_{\eta_r}^{\eta_0} d\eta (\dot{\Psi} - \dot{\Phi}) j_l[k(\eta_0 - \eta)]. \tag{43}$$

Furthermore, one can assume that the tight coupling regime effectively never ended at the time of recombination, which requires us to make the approximation $\eta_r \approx \epsilon$ (and $\eta_* = 0$). This is clearly not totally true, since recombination of the protons and electrons did take place, but the only thing critical for estimating the anisotropies is the visibility. In the specific case of *shifted* last scattering which we are considering here, the visibility of the time of recombination is almost negligible. Therefore, we can estimate

$$\hat{\Delta}_0(\eta_r) = \Delta_0(\eta_r) + \Phi(\eta_r)$$

$$= e^{-k^2/k_s^2(\eta_r,0)} \left[\hat{\Delta}_0(0) \cos\left(\frac{k\eta_r}{\sqrt{3}} \right) \right.$$

$$+ \frac{\sqrt{3}}{k} \dot{\hat{\Delta}}_0(0) \sin\left(\frac{k\eta_r}{\sqrt{3}} \right) \right] + \sqrt{\frac{3}{k}} \int_0^{\eta_r} d\eta' e^{-k^2/k_s^2(\eta_r,\eta')}$$

$$\times \sin\left(\frac{k}{\sqrt{3}} (\eta_r - \eta') \right) F(\eta'). \tag{44}$$

We see now that there is just one set of peaks with their scale set by $k_r \sim \eta_r^{-1}$. Since $\eta_r \gg \eta_*$, this corresponds to a shift of the entire peak structure to smaller l. Also the diffusion damping length $k_s^{-1}(\eta_r, 0)$ has grown considerably and hence the effects of Silk damping [88] are prevalent on larger scales than in the standard scenario [86].

We could also use this limit to understand the effects of *delayed* recombination, since there is just one surface of last scattering, but it seems more logical to treat this case as its name suggests as an increase in η_*, with $\tau(\eta_r) = 0$. This leads to a simple shift in the time of recombination, and hence the size of the sound horizon when the photons last scatter. The observational consequence is that the whole spectrum of anisotropies and also the Silk damping envelope are shifted to larger scales.

The effects of these modified thermal histories on the position of peaks in the polarization is very similar to their effects on the temperature anisotropy. This is since the evolution of the source of polarization inside any surface of last scattering induced by reionization is very much the same as in the standard case. Therefore, if we make the same assumptions about the surface of last scattering, then the polarization is given by [20]

$$E_l(k, \eta_0) = -\sqrt{6} \{ e^{-\tau(\eta_r)} P(\eta_*) \epsilon_l[k(\eta_0 - \eta_*)] $$
$$+ (1 - e^{-\tau(\eta_r)}) P(\eta_r) \epsilon_l[k(\eta_0 - \eta_r)] \}. \tag{45}$$

As for the anisotropy, the function $\epsilon_l(x) \propto j_l(x)$ peaks around $l \approx x$ and the two contributions to (45) produce peaks on the two scales $l \approx k_*(\eta_0 - \eta_*)$ and $l \approx k_r(\eta_0 - \eta_r)$. Similar shifts in the peak position are possible in the cases of *shifted* and *delayed* last scattering. Since the polarization has only one source, as opposed to the temperature which has a number, this effect will be seen much more clearly.

However, the amplitude of polarization on different scales is much more difficult to understand in any kind of generality. First, there are effects of Silk damping, which are likely to be very much the same as for the anisotropy. But more importantly there is the added difficulty of pre-existing polarization at the time of reionization. In the standard case, the quadrupole is negligible until very close to the time of last scattering and so its amplitude increases during that time, while oscillating out of phase with the monopole. It is the balance between this increase and the effects of Silk damping which makes the amplitude maximum at around the third or fourth peak. If the quadrupole is nonzero before the time of reionization, as is likely to be the case particularly in the *double* last scattering scenario, then it is possible to shift this balance to larger scales. Hence, it is possible for the maximum amplitude to be at the first peak.

It is hard to obtain any analytical predictions for the total ionization model. This is because the last scattering visibility function is smeared out over the whole history since recombination and cannot be approximated by a simple function with two peaks (Fig. 5). Therefore the line of sight integrals (31), (33) cannot be carried out in a simple way. The only prediction we can make is, since this scenario gives a small cumulative visibility up to very late times (see Fig. 5, last scattering visibility function), that the resulting anisotropy power spectrum will be suppressed up to relatively large scales.

B. Isocurvature white noise

Our main emphasis in this paper is on active source models. However, there is a class of passive models, known as isocurvature white-noise models, which have a number of the features of an active model. We have integrated the linearized Einstein-Boltzmann equations with an integrator known as CMBFAST [34] for an isocurvature cold dark matter (CDM) model [90–92] with the initial power spectrum
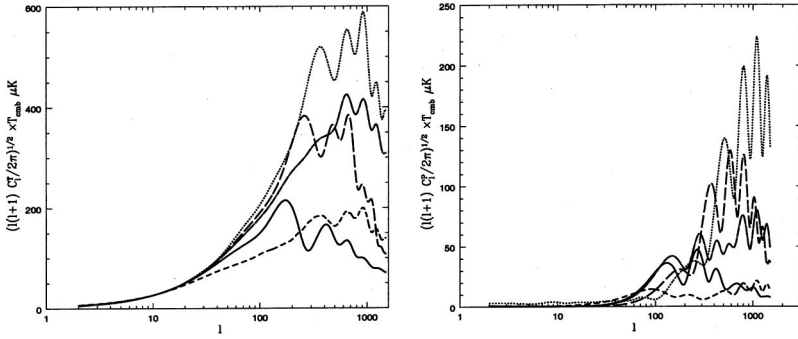
$$P_i(k) = k^0, \tag{46}$$

FIG. 7. The temperature (left) and polarization (right) anisotropy power spectra for an isocurvature CDM model. The dotted line refers to the standard thermal history, the long dashed line to delayed last scattering, the solid line to shifted last scattering, the dot-dashed line to double last scattering, and the short dashed line to the total ionization scenario.

that is, an initial white-noise spectrum and the results for our sample of modified thermal histories discussed in the previous section are shown in Fig. 7. The power spectrum is plotted up to $l=1500$, because we do not expect interesting features on smaller scales in this first order approach. We should note first that, for the standard thermal history, the amplitude and spectrum of such a model is very much in conflict with the current observations [93]. However, as we shall discuss in Sec. III D, part of the motivation for this work is to investigate how the changes in the ionization history might create a more acceptable model.

We see that the peak structure in the delayed and shifted last scattering scenarios is moved to much larger scales and that amplitude is suppressed by the damping envelope, very much in keeping with the analytic arguments of the previous section. For the case of double last scattering the analytic treatment suggests that there should be a second set of peaks at larger scales, but it appears that in this particular case that this second set of peaks is suppressed below that of the first set. The first peak which appears for the standard case at $l \approx 350$ also appears to be ''washed'' out by the damping at the time of reionization. However, the three peaks which remain are on exactly the same scales as those in the standard case and represent the anisotropy created at the time of the initial epoch of recombination, suppressed by the damping factor $e^{-\tau(\eta_r)}$. Finally the total ionization scenario results in a heavy suppression of power up to very large scales ($l \approx 20$). This is because the last scattering visibility function is smeared out over the whole time since recombination (Fig. 5). We should note that reionization only appears to be effective on small scales and in each case the anisotropy on scales with $l<20$ remains unchanged.

As already discussed the peak structure of the polarization power spectrum is a more clean test of our analytic arguments, although our understanding of the amplitude is much less clear. In the standard case, the first peak is around $l \approx 250$ and the damping becomes effective on scales with $l >1000$. Once again the action of the delayed and shifted last scattering is easily understood from our analytic arguments with just a universal shift of the spectrum and damping scales. In the double last scattering scenario we now see that there are two clear sets of peaks which have different scales, those at the smaller scales being those created at the time of recombination damped by the appropriate amount. Since the visibility function at recombination is not completely zero, the damping phase leads to a quadrupole moment in the temperature anisotropies. This quadrupole contribution acts as a

seed for the creation of polarization anisotropies (33) during reionization and hence the first peak in the polarization for this model is more prominent than in the others. Finally, total ionization results in a severely damped polarization spectrum, although even in this very extreme case one can just observe the remnants of the polarization created at the standard time of recombination.

C. Simple coherent scaling source models

In order to study active sources we will first discuss the simple coherent scaling source models introduced in Refs. [94,95]. Although these kind of sources are unlikely to be realized in the early universe, they have some some illustrative value. The scaling source is introduced as components of the Newtonian metric perturbations; specifically the curvature $\Phi = \Phi_{\gamma b} + \Phi_s$ and the gravitational potential $\Psi = \Psi_{\gamma b} + \Psi_s$, where $\Phi_{\gamma b}$ and $\Psi_{\gamma b}$ are the contributions from the photon-baryon fluid, and Φ_s and Ψ_s are those for the source. These sources terms can be related to the density of the source ρ_s, its velocity v_s and anisotropic stress π_s by [95]

$$k^2 \Phi_s = 4\pi G a^2 \left(\rho_s + 3\frac{\dot{a}}{a} v_s/k \right),$$
$$k^2 (\Psi_s + \Phi_s) = -8\pi G a^2 \pi_s, \tag{47}$$

where the derivatives are with respect to conformal time $\eta = \int dt/a$. The conservation equations for the seed source are [95]

$$\dot{\rho}_s + 3\frac{\dot{a}}{a}(\rho_s + p_s) = -k v_s,$$
$$\dot{v}_s + 4\frac{\dot{a}}{a} v_s = k p_s - \frac{2}{3} k \pi_s, \tag{48}$$

where p_s is the pressure of the source. Clearly, there are only two independent quantities here and we can in general choose any two arbitrarily, the other two being computed by evolving these equations. One simple scaling ansatz, which we shall call the pressure source, is given by [95]

$$4\pi G a^2 p_s = \eta^{-1/2} \frac{\sin(A k \eta)}{A k \eta},$$
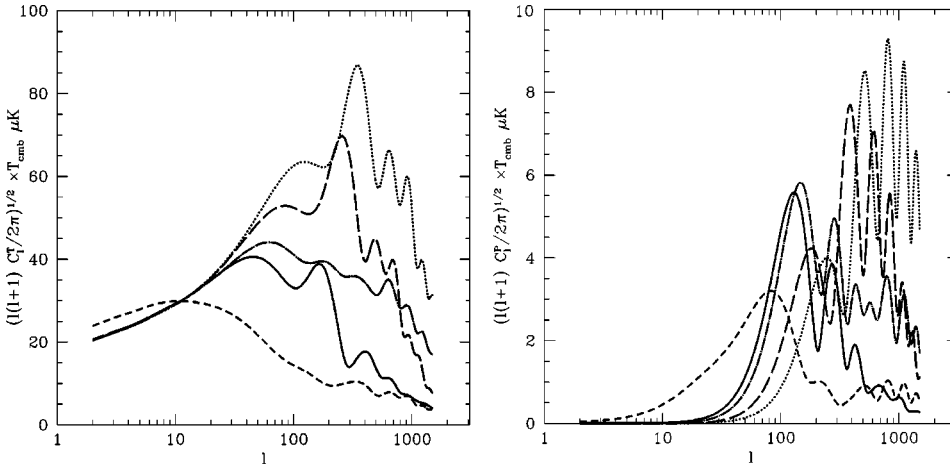$$\pi_s = 0, \tag{49}$$

FIG. 8. Temperature (left) and polarization (right) anisotropy power spectra for a pressure source model with $A = 1.0$. The dotted line refers to the standard thermal history, the long dashed line to delayed last scattering, the solid line to shifted last scattering, the dot-dashed line to double last scattering, and the short dashed line to the total ionization scenario.

where $0 < A < 1$ and another which we shall call the stress source has

$$4\pi G a^2 \pi_s = \eta^{-1/2} \frac{6}{B_2^2 - B_1^2} \left[\frac{\sin(B_1 k \eta)}{B_1 k \eta} - \frac{\sin(B_2 k \eta)}{B_2 k \eta} \right],$$
(50)

where $0 < (B_1, B_2) < 1$, with p_s given by the pressure source. For the results presented here we have chosen to use $A = 1.0$, $B_1 = 1.0$ and $B_2 = 0.5$.

Figures 8 and 9 show the results of incorporating the pressure and stress sources into CMBFAST. For the pressure source the anisotropy results follow the exact pattern predicted by our analytic arguments and already confirmed in the isocurvature white noise model. Now the main contribution to the intrinsic anisotropy is from the third term of the tight coupling solution (37), which moves the dominant peak in the temperature anisotropy to smaller scales. The delayed and shifted scenarios comprise a single set of peaks at larger scales than in the standard case, and in particular the main peak, which is at around $l \approx 350$ in the standard case, is moved to around $l \approx 250$ in the delayed scenario. In the case of *double last scattering* one can still recognize the peaks from the recombination epoch on small scales. However the expected second set of peaks from reionization is hardly recognizeable. The polarization in each of these cases also follows the pattern already established.

One should note that in these truly active models the large-scale anisotropy is created by the ISW effect due to the existence of the sources along the line of sight. In the delayed, shifted and double last scattering scenarios reionization takes place very much before $z \approx 100$, whereas most of the ISW effect comes from sources present after this time. Therefore, reionization has very little impact on this contribution, that is, the penultimate term in (40) is effectively zero. In the total ionization scenario, where the universe is ionized for most of the time between standard last scattering and the present day, this is not necessarily the case and reionization can interfere with the anisotropy on large scales. This is illustrated in Fig. 8, although superficially it appears that the large-angle contribution has increased. This is not in fact the case since the normalization to COBE makes all the models equally around $l = 10$. What has happened is a redistribution of the large-scale power and a reduction of the contribution to the COBE normalization from scales smaller than $l \approx 10$. This will not always be the case since it depends critically on the time when most of the anisotropy is created relative to the ionization history.

The results of using the stress source are very similar to those from the pressure source as illustrated in Fig. 9. How-
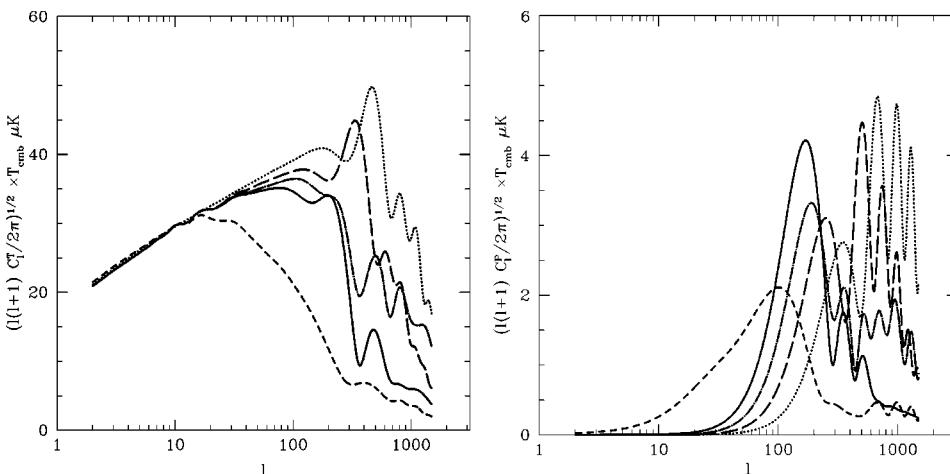

FIG. 9. Temperature (left) and polarization (right) anisotropy power spectra for a stress source model with $A = 1.0$, $B_1 = 1.0$ and $B_2 = 0.5$. The key to the curves is the same as in Fig. 8.

ever, there is one case which is quantitatively different. It appears that the first peak in the polarization spectrum for the shifted scenario is higher than that for the double last scattering scenario, where in the two cases already considered (the isocurvature white noise and pressure models) these peaks have almost the same height. We believe that this subtle effect is due to the quadrapole of the temperature anisotropy, which is the source for polarization, being non-zero when the second tight-coupling epoch begins, although we have no analytic reasoning for this.

D. Causal white noise

One of the original motivations for studying these non-standard thermal histories was to attempt to rectify some of the observational problems of a class of structure formation models known as causal white noise (CWN) models [96,97]. These models were spawned out of the realization that standard scaling models with defect motivated stress-energy components are unable to explain the observed matter fluctuations on $100h^{-1}$ Mpc scales in a Einstein-de-Sitter universe, unless in case where large scale biases are acceptable. It was suggested that if the source was switched off at some point before a critical redshift ($z_c \approx 100$), then the power on $100h^{-1}$ Mpc scales was exactly that observed and the excess of power on smaller scales can be rectified by modifications to cosmological parameters. An observationally unacceptable side-effect of this is the spectrum of CMB anisotropies produced.

Figure 10 illustrates these problems for a simple CWN model in the standard thermal history, plus the effects of our total ionization scenario, in both an Einstein-de-Sitter cosmology and also one with a non-zero cosmological constant. In the standard scenario we see that there appears to be an excess of power on small scales and the shape of the spectrum on large scales is in conflict with the COBE data. This is because these models effectively tilt the spectrum toward smaller scales. The action of reionization is to reduce the power on small scales to a more acceptable level, but the problems on large-scales remain. These can be partially relieved by the inclusion of a cosmological constant, but at the expense of reducing the power on smaller scales. It was concluded in Refs. [96,97] that although such models can explain the formation of structure, they have considerable problems explaining the observed CMB power spectrum.

E. Cosmic strings with a cosmological constant

The other motivation is to investigate whether acoustic peaks in defect models may shift to larger angular scales in realistic thermal histories. We have already mentioned that these models appear to predict a peak (if any at all, see Refs. [24–26,30]) on much smaller scales than in the standard adiabatic scenario, and in fact only very convoluted models can rectify this [94]. One might ask is this a generic phenomena and clearly our earlier arguments suggest that the ionization history can be modified to allow this to happen in more generic defect models.

We have applied the same modified thermal histories to the model of structure formation by cosmic strings with a
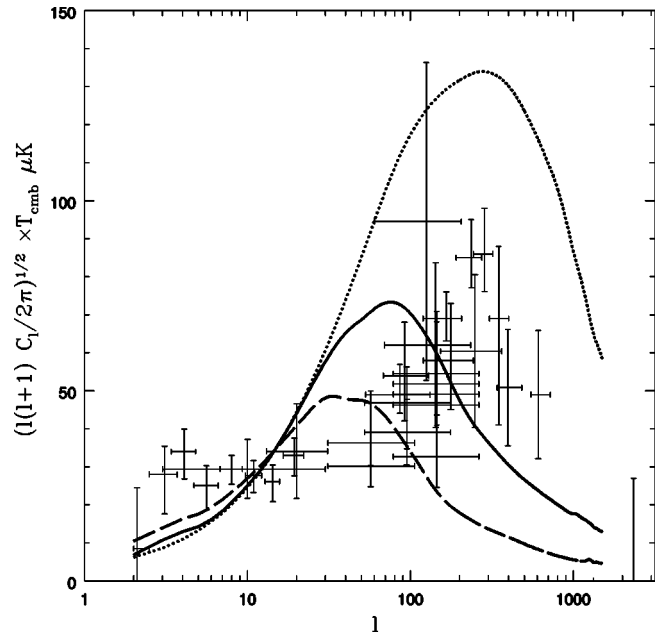

FIG. 10. Temperature anisotropy power spectrum for a causal white noise model. The dotted line is for a standard thermal history, the solid line for a total ionization history with the parameters $\bar{z} = 400$, $\rho = 350$ and $T_{\text{heat}} = 3 \times 10^7$ K and the long dashed line is for the same model with inclusion of a cosmological constant $\Omega_\Lambda = 0.65$, $\Omega_b = 0.1$ and $\Omega_c = 0.25$. The spectra include scalar, vector and tensor contributions and are normalized to COBE. Also included are the observations data points [98].

cosmological constant presented in Ref. [29]. The introduction of a non-zero cosmological constant can improve the shape of the matter power spectrum and its amplitude on scales of $100h^{-1}$ Mpc to an acceptable level, and it was shown that an important consequence of this is a broad peak in the CMB power spectrum on around $l = 500$. The model presented here has $\Omega_B = 0.05$, $\Omega_c = 0.15$ and $\Omega_\Lambda = 0.80$. In Fig. 11 we have plotted the temperature anisotropy power spectrum for our thermal histories with this model. The spectrum behaves very much as one might have expected from our earlier analytic arguments and also like the simple coherent models, although it should be noted that in this incoherent model the concept of peaks is slightly different. For standard recombination (dotted line) the peak is at $l \approx 500$ and has an amplitude of ≈ 95 μK, which has been shifted, for example, in the case of *double* last scattering (dot-dashed line) to a broader peak at $l \approx 200$ and a height of 60 μK. Similar modifications are made in the shifted and delayed last scattering scenarios. This is clearly an improvement with respect to the current observational data, although maybe not a necessary one.

IV. DISCUSSION AND CONCLUSION

We have introduced a heating source motivated by the *active* character of structure formation in the context of sources like a cosmic strings. The main assumption is that there exists a phase in the universe after recombination, where the density of active sources is large enough to heat
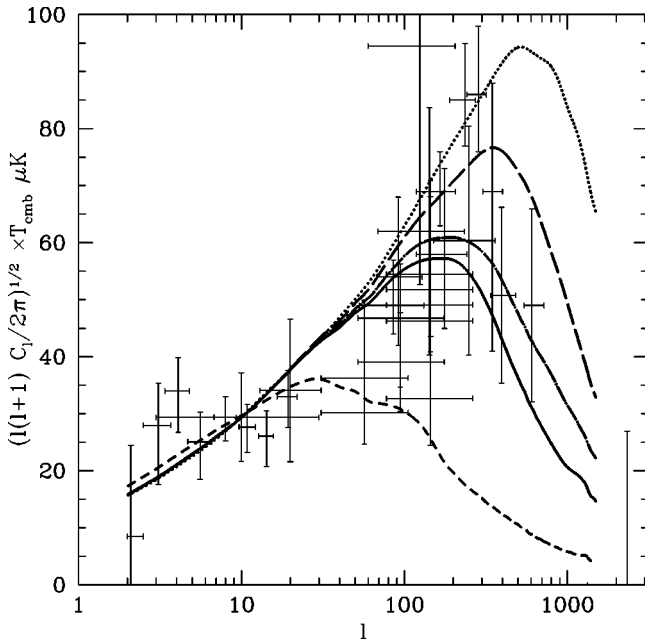
FIG. 11. The temperature anisotropy power spectra for a cosmic string model under inclusion of a cosmological constant Ω_Λ $=0.80$. The key of the plot is the same as in Fig. 7. We have also included the data points with errorbars [98].

the baryons *homogenously*, at least over a short period of time. After this the influence of the active sources on the heating was assumed to be irrelevant for our effective description. Sources of ''late'' reionization, such as, photoionization through early object formation are not included in our analysis. We also have not considerd the second order contribution from the Vishniac effect [99,100], which will lead to an extra contribution in the temperature anisotropy power spectrum at large l ($l>2000$). An inhomogenous treatment would also have led to such second order contributions [101].

We calculated the spectral distortions for a wide range of heat source parameters and established that it is hard to violate the COBE FIRAS limits on these quantities. We extended the framework of the semi-analytical Hu and Sugiyama formalism [77] to the case of reionization and analyzed four generic heat source types explaining their influence on the CMB temperature anisotropy and polarization power spectra for isocurvature white noise and simple scaling source models. The behavior of the models was explained well by these arguments. We have found that if there is only a shift of the surface of last scattering, the anisotropy power spectrum becomes damped and the peaks are shifted to larger scales. If there appears a second surface of last scattering the acoustic peak structure changes and the suppression on small scales is not as large for a just shifted last scattering surface. The most important feature of the polarization power spectrum is the appearance of a prominent contribution on intermediate scales due to reionization. We then applied the source models to CWN models and also to a realistic cosmic string model. We found that it was possible to reduce the amount of power on small scales in CWN models and to move the peak in string models to larger scales — the original motivation for this work. However, it appears to not be possible to have a substantial effect on the spectrum at large angles in CWN models.

[1] N. Kaiser, Astrophys. J. **282**, 374 (1984).
[2] N. Vittorio and J. Silk, Astrophys. J. Lett. **285**, L39 (1984).
[3] J.R. Bond and G. Efstathiou, Astrophys. J. Lett. **285**, L45 (1984).
[4] H.M.P. Couchman and M.J. Rees, Mon. Not. R. Astron. Soc. **221**, 53 (1986).
[5] E.I. Dorosheva and P.D. Nasel'skij, Astrophys. **24**, 321 (1986).
[6] J.R. Bond, G. Efstathiou, P.M. Lubin, and P.R. Meinhold, Phys. Rev. Lett. **66**, 2179 (1991).
[7] N. Sugiyama, J. Silk, and N. Vittorio, Astrophys. J. Lett. **419**, L1 (1993).
[8] W. Hu, D. Scott, N. Sugiyama, and M. White, Phys. Rev. D **52**, 5498 (1995).
[9] J.E. Gunn and B.A. Peterson, Astrophys. J. **142**, 1633 (1965).
[10] J. Miralda-Escudé and J.P. Ostriker, Astrophys. J. **350**, 1 (1990).
[11] M. Tegmark, J. Silk, and A. Blanchard, Astrophys. J. **420**, 484 (1994).
[12] R. Durrer, Infrared Phys. Technol. **35**, 83 (1994).
[13] M. Fukugita and M. Kawasaki, Mon. Not. R. Astron. Soc. **269**, 563 (1994).
[14] A.R. Liddle and D.H. Lyth, Mon. Not. R. Astron. Soc. **273**, 1177 (1995).
[15] J. Arons and D.W. Wingert, Astrophys. J. **177**, 1 (1972).
[16] P.R. Shapiro and M.L. Giroux, Astrophys. J. Lett. **321**, L107 (1987).
[17] A. Meiksin and P. Madau, Astrophys. J. **412**, 34 (1993).
[18] P.R. Shapiro, M.L. Giroux, and A. Babul, Astrophys. J. **427**, 25 (1994).
[19] Z. Haiman and A. Loeb, Astrophys. J. **483**, 21 (1997).
[20] M. Zaldarriaga, Phys. Rev. D **55**, 1822 (1997).
[21] Ya.B. Zel'dovich, Mon. Not. R. Astron. Soc. **192**, 663 (1980).

[22] A. Vilenkin, Phys. Rev. Lett. **46**, 1496 (1981).

[23] N. Tuork and D.N. Spergel, Phys. Rev. Lett. **64**, 2736 (1989).

[24] U.L. Pen, U. Seljak, and N. Turok, Phys. Rev. Lett. **79**, 1615 (1997).

[25] A. Albrecht, R.A. Battye, and J. Robinson, Phys. Rev. Lett. **79**, 4736 (1997).

[26] A. Albrecht, R.A. Battye, and J. Robinson, Phys. Rev. D **59**, 023508 (1999).

[27] C. Contaldi, M. Hindmarsh, and J. Magueijo, Phys. Rev. Lett. **82**, 679 (1999).

[28] L. Pogosian and T. Vachaspati, Phys. Rev. D **60**, 083504 (1999).

[29] R.A. Battye, J. Robinson, and A. Albrecht, Phys. Rev. Lett. **80**, 4847 (1997).

[30] B. Allen, R.R. Caldwell, S. Dodelson, L. Knox, E.P.S. Shellard, and A. Stebbins, Phys. Rev. Lett. **79**, 2624 (1997).

[31] P.P. Avelino, E.P.S. Shellard, J.H.P. Wu, and B. Allen, Phys. Rev. Lett. **81**, 2008 (1998).

[32] P.P. Avelino, R.R. Caldwell, and C.J.A.P. Martins, Phys. Rev. D **56**, 4568 (1997).

[33] A. Sornborger, R. Brandenberger, B. Fryxell, and K. Olson, Astrophys. J. **482**, 22 (1997).

[34] U. Seljak and M. Zaldarriaga, Astrophys. J. **469**, 437 (1996).

[35] P.J.E. Peebles, Astrophys. J. **153**, 1 (1968).

[36] Ya.B. Zel'dovich, V.G. Kurt, and R.A. Sunyaev, Zh. Éksp. Teor. Fiz. **55**, 278 (1968) [Sov. Phys. JETP **28**, 146 (1969)].

[37] S. Seager, D.D. Sasselov, and D. Scott, Astrophys J. (to be published).

[38] C.P. Ma and E. Bertschinger, Astrophys. J. **455**, 7 (1995).

[39] P.J.E. Peebles, *Principles of Physical Cosmology* (Princeton University Press, Princeton, NJ, 1993).

[40] R.J. Gould and R.K. Thakur, Ann. Phys. (N.Y.) **61**, 351 (1970).

[41] G.R. Burbidge, R.J. Gould, and S.R. Pottasch, Astrophys. J. **138**, 945 (1963).

[42] M. Rees (private communication).

[43] A.S. Kompaneets, Zh. Éksp. Teor. Fiz. **31**, 876 (1957) [Sov. Phys. JETP **4**, 730 (1957)].

[44] Ya.B. Zeldovich and R.A. Sunyaev, Astrophys. Space Sci. **4**, 301 (1969).

[45] R.A. Sunyaev and Ya.B. Zeldovich, Astrophys. Space Sci. **7**, 20 (1969).

[46] K.L. Chan and B.J.T. Jones, Astrophys. J. **195**, 1 (1975).

[47] A.P. Lightman, Astrophys. J. **244**, 392 (1981).

[48] P. Salati and J.C. Wallet, Phys. Lett. B **144**, 61 (1984).

[49] X. Asselin, G. Girardi, P. Salati, and A. Blanchard, Nucl. Phys. **B310**, 669 (1987).

[50] D.W. Sciama and A.L. Melott, Phys. Rev. D **25**, 2214 (1982).

[51] D.W. Sciama, Mon. Not. R. Astron. Soc. **198**, 1P (1982).

[52] D. Scott, M.J. Rees, and D.W. Sciama, Astron. Astrophys. **250**, 295 (1991).

[53] P.D. Nasel'skij and A.G. Polonarëv, Pis'ma Astron. Zh. **13**, 167 (1987) [Sov. Astron. Lett. **13**, 67 (1987)].

[54] R. Weymann, Astrophys. J. **145**, 560 (1966).

[55] C. Burigana, G. de Zotti, and L. Danese, Astron. Astrophys. **303**, 323 (1995).

[56] L. Danese and G. de Zotti, Riv. Nuovo Cimento **7**, 277 (1977).

[57] A. Stebbins and J. Silk, Astrophys. J. **300**, 1 (1986).

[58] R. Weymann, Phys. Fluids **8**, 2112 (1965).

[59] J.G. Bartlett and A. Stebbins, Astrophys. J. **371**, 8 (1991).

[60] G. Smoot, in *Proceedings of the NATO Advanced Study Institute on The Cosmic Microwave Background*, Strasbourg, France, edited by C.H. Lineweaver *et al.* (Kluwer Academic, Boston, 1997).

[61] W. Hu and J. Silk, Phys. Rev. D **48**, 485 (1993).

[62] G.B. Rybicki and A.P. Lightman, *Radiative Processes in Astrophysics* (Wiley, New York, 1979).

[63] M.B. Entel, P.D. Nasel'skij, and V.N. Lukash, Nuovo Cimento B **89**, 47 (1985).

[64] See the MAP homepage at: http://map.gsfc.nasa.gov/

[65] See the Planck Surveyor homepage at: http://astro.estec.esa.nl/SA-general/Projects/Planck/

[66] M. Bersanelli *et al.*, Phase A study for the *Cobras/Samba* Mission. Paris: European Space Agency D/SCI(96)3 (1996).

[67] See the DIMES homepage at: http://ceylon.gsfc.nasa.gov/DIMES/

[68] A. Kogut, in *Proceedings of the XVI Moriond Astrophysics meeting*, Les Arcs, France, edited by J. Trân Thanh Vân *et al.* (Editions Frontiers, Paris, 1996).

[69] A. Stebbins, in *Proceedings of the NATO Advanced Study Institute on The Cosmic Microwave Background* (Ref. [60]).

[70] P.J.E. Peebles and J.T. Yu, Astrophys. J. **162**, 815 (1970).

[71] M.L. Wilson and J. Silk, Astrophys. J. **243**, 14 (1981).

[72] A.G. Doroshkevich, Ya.B. Zel'dovich, and R.A. Sunyaev, Astron. Zh. **55**, 913 (1978) [Sov. Astron. **22**, 523 (1978)].

[73] A.G. Doroshkevich, Pis'ma Astron. Zh. **14**, 296 (1988) [Sov. Astron. Lett. **14**, 125 (1988)].

[74] P.D. Nasel'skij and I. Novikov, Astrophys. J. **413**, 14 (1993).

[75] F. Atrio-Barandela and A.G. Doroshkevich, Astrophys. J. **420**, 26 (1994).

[76] H.E. Jǿrgensen, E. Kotok, P.D. Nasel'skij, and I. Novikov, Astron. Astrophys. **294**, 639 (1995).

[77] W. Hu and N. Sugiyama, Astrophys. J. **444**, 489 (1995).

[78] W. Hu and N. Sugiyama, Phys. Rev. D **51**, 2599 (1995).

[79] M. Zaldarriaga and D.D. Harari, Phys. Rev. D **52**, 3276 (1995).

[80] W. Hu and M. White, Phys. Rev. D **56**, 596 (1997).

[81] J. Magueijo, A. Albrecht, D. Coulson, and P. Ferreira, Phys. Rev. Lett. **76**, 2617 (1996).

[82] J. Magueijo, A. Albrecht, P. Ferreira, and D. Coulson, Phys. Rev. D **54**, 3727 (1996).

[83] R.A. Battye, Phys. Rev. D **55**, 7361 (1997).

[84] W. Hu, U. Seljak, M. White, and M. Zaldarriaga, Phys. Rev. D **57**, 3290 (1998).

[85] K.L. Ng and K. Ng, Phys. Rev. D **51**, 364 (1995).

[86] W. Hu and M. White, Astrophys. J. **479**, 568 (1997).

[87] U. Seljak and M. Zaldarriaga, Phys. Rev. Lett. **78**, 2054 (1997).

[88] J. Silk, Astrophys. J. **151**, 459 (1968).

[89] W. Hu and M. White, Astrophys. J. **471**, 30 (1996).

[90] A.D. Linde, Phys. Lett. **158B**, 375 (1985).

[91] D. Seckel and M.S. Turner, Phys. Rev. D **32**, 3178 (1985).

[92] P.J.E. Peebles, Astrophys. J. Lett. **483**, L1 (1997).

[93] W. Hu, E.F. Bunn, and N. Sugiyama, Astrophys. J. Lett. **447**, L59 (1994).

[94] N. Turok, Phys. Rev. D **54**, R3686 (1996).

[95] W. Hu, D.N. Spergel, and W. White, Phys. Rev. D **55**, 3288 (1997).

[96] A. Albrecht, in *Proceedings of the International Workshop on Particle Physics and the Early Universe*, Ambleside, edited by L. Roszkowski (World Scientific, New Jersey, 1998).

[97] A. Albrecht, R.A. Battye, J. Robinson and J. Weller (in preparation).

[98] The data points have been compiled by M. Tegmark at http://www.sns.ias.edu/~max/cmb/experiments.html

[99] E. Vishniac, Astrophys. J. **322**, 597 (1987).

[100] S. Dodelson and J.M. Jubas, Astrophys. J. **439**, 503 (1995).

[101] W. Hu and A. Gruzinov, Astrophys. J. **508**, 435 (1998).